Ultrafast demagnetization mechanism in half-metallic Heusler alloy thin films controlled by the Fermi level

Santanu Pan,[1] Takeshi Seki,[2,3] Koki Takanashi,[2,3,4] and Anjan Barman[1,*]

[1]*Department of Condensed Matter Physics and Material Sciences, S. N. Bose National Centre for Basic Sciences, Block JD, Sector III, Salt Lake, Kolkata 700 106, India*

[2]*Institute for Materials Research, Tohoku University, Sendai 980-8577, Japan*

[3]*Center for Spintronics Research Network, Tohoku University, Sendai 980-8577, Japan*

[4]*Center for Science and Innovation in Spintronics, Core Research Cluster, Tohoku University, Sendai 980-8577, Japan*

(Received 14 December 2019; revised manuscript received 21 May 2020; accepted 21 May 2020; published 8 June 2020)

The electronic band-structure controlled ultrafast demagnetization mechanism in $Co_2Fe_xMn_{1-x}Si$ Heusler alloy is underpinned by systematic variation of composition. We find the spin-flip scattering rate controlled by spin density of states at the Fermi level is responsible for nonmonotonic variation of ultrafast demagnetization time (τ_M) with x with a maximum at $x = 0.4$. Furthermore, Gilbert damping constant exhibits an inverse relationship with τ_M due to the dominance of interband scattering mechanism. This demonstrates a connection between ultrafast demagnetization and magnetic damping based on Fermi-level position in this Heusler alloy system.

DOI: 10.1103/PhysRevB.101.224412

I. INTRODUCTION

The tremendous application potential of spin-polarized Heusler alloys in advanced spintronics devices ignites immense interest to investigate the degree and sustainability of their spin polarization under various conditions [1–4]. Heusler alloys belong to a special class of material known as half metals, e.g., CrO_2, La-Sr-Mn-O, etc., which have very low minority spin density of states (MSDOS) at the Fermi level and thus they possess very high spin polarization. For these materials, the demagnetization time slows down due to a minority state-blocking effect. Depending on the degree of spin polarization, the demagnetization time in these systems ranges from 100 fs to 100 ps. On the other hand, interpretation of spin polarization from the conventional methods such as photoemission, spin transport measurement, point-contact Andreev reflection, and spin-resolved positron annihilation are nontrivial [5–7]. In the quest of developing alternative methods, Zhang *et al.* demonstrated that all-optical ultrafast demagnetization measurement is a reliable technique for probing spin polarization [8]. They observed a very large ultrafast demagnetization time as a signature of high spin polarization in half-metallic CrO_2. However, Co-based half-metallic Heusler alloys exhibit a comparatively smaller ultrafast demagnetization time ($\sim$0.3 ps) which raised a serious debate on the perception of ultrafast demagnetization mechanism in Heusler alloys [9–11]. A smaller demagnetization time in Heusler alloys than in CrO_2 is explained due to the smaller effective band gap in the minority spin band and enhanced spin-flip scattering (SFS) rate [9]. However, earlier investigations did not consider any excitation in the minority band and further experimental evidence shows that the amount of band gap in a minority spin band cannot be the only deciding factor for SFS-mediated ultrafast demagnetization efficiency [10]. Rather, one also has to consider the efficiency of optical excitation for majority and minority spin bands as well as the optical pump-induced hole dynamics below Fermi energy (E_F). Consequently, a clear interpretation of spin polarization from ultrafast demagnetization measurement requires a clear and thorough understanding of its underlying mechanism. Since its inception in 1996 [12], several theoretical models and experimental evidence based on different microscopic mechanisms, e.g., SFS and superdiffusive spin current, have been put forward to interpret ultrafast demagnetization [13–20] which continues to the most recent proposal of the optically induced spin transfer (OISTR) effect [21,22]. However, the preceding proposals are complex, which increases even more in the case of a special class of material such as the Heusler alloys. The position of Fermi level can be greatly tuned by tuning the alloy composition of Heusler alloys [23,24]. By utilizing this tunability, here, we experimentally demonstrate that the ultrafast demagnetization mechanism relies on the spin density of states at the Fermi level in the case of half-metallic Heusler alloy system. We extracted the value of ultrafast demagnetization time using three-temperature modeling [25] and found its nonmonotonic dependency on alloy composition (x). We have further shown that the Gilbert damping constant and ultrafast demagnetization time are inversely proportional in $Co_2Fe_xMn_{1-x}Si$ (CFMS) Heusler alloys, suggesting the interband scattering as the primary mechanism behind the Gilbert damping in CFMS Heusler alloys. Our work has demonstrated a correlation in between the ultrafast demagnetization time and the Gilbert damping constant.

*abarman@bose.res.in

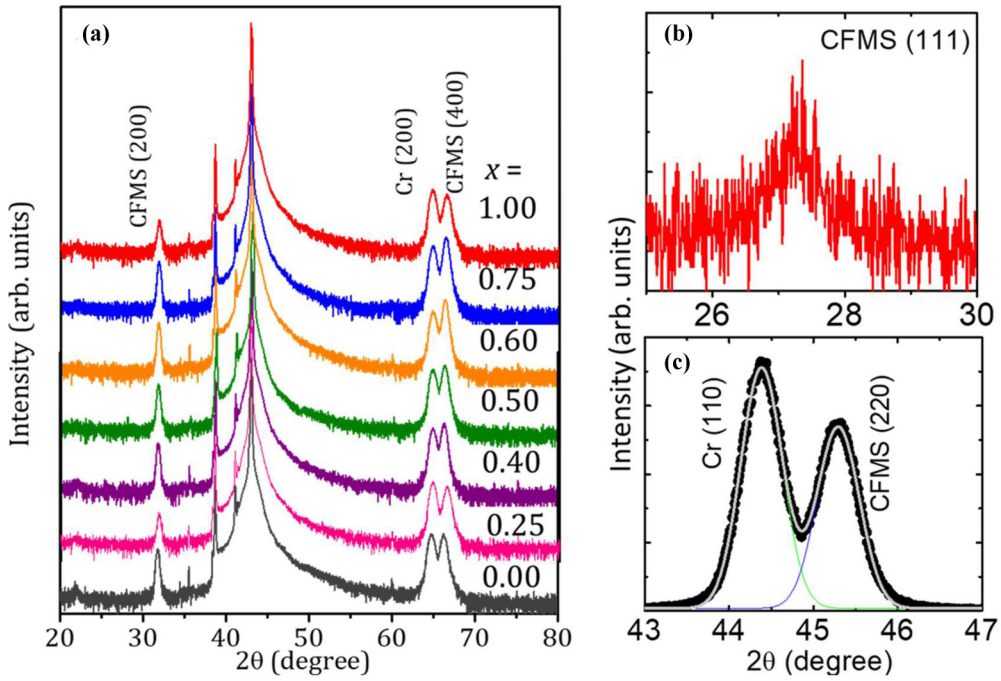

FIG. 1. (a) XRD patterns of $Co_2Fe_xMn_{1-x}Si$ thin films for different alloy composition (x) measured in conventional θ-2θ geometry. Both CFMS (200) superlattice and CFMS (400) fundamental peaks are marked along with Cr (200) peak. (b) The tilted XRD patterns reveal the CFMS (111) superlattice peak for $L2_1$ structure. (c) CFMS (220) fundamental peak together with Cr (110) peak.

II. RESULTS AND DISCUSSION

A series of CFMS thin films have been deposited using a magnetron cosputtering system for our investigation with $x = 0.00, 0.25, 0.40, 0.50, 0.60, 0.75$, and 1.00 on Cr-buffered MgO substrate [26,27]. The thickness of the CFMS layer was fixed at 30 nm. It is imperative to study the crystalline phase, which is the most crucial parameter that determines other magnetic properties of Heusler alloy. Thus, prior to the magnetization dynamics measurement, we have investigated both the crystalline phase as well as growth quality of all the samples. Figure 1(a) shows the *ex situ* x-ray diffraction (XRD) pattern for all the samples. The well-defined diffraction peak of CFMS (400) at $2\theta = 66.50^\circ$ indicates that the samples are well crystalline having cubic symmetry. The intense superlattice peak at $2\theta = 31.90^\circ$ represents the formation of $B2$ phase. The presence of other crucial planes are investigated by tilting the sample $x = 0.4$ by 54.5° and 45.2° from the film plane to the normal direction, respectively, and observing the presence of (111) superlattice peak along with the (220) fundamental peak as shown in Figs. 1(b) and 1(c). The presence of (111) superlattice peak confirms the presence of $L2_1$ atomic site ordering, whereas the (220) fundamental peak results from the cubic symmetry. However, we do not observe the $L2_1$ peak for $x = 0.25$ sample, probably because of degraded structural quality for this sample. The intensity ratios of the XRD peaks are analyzed to obtain the microscopic atomic site ordering which remains same for the whole range of x (given in Supplemental Materials [28]). Although we find that the degree of $L2_1$ ordering (∼20%) is moderate as compared to the high degree of $B2$ ordering (∼80%), the latter ensures the occurrence of half metallicity for the present samples (shown in Supplemental Materials [28]) [29]. The epitaxial growth of the thin films is also ensured from the *in situ* reflection high-energy electron diffraction (RHEED) images. The square-shaped hysteresis loops obtained using in-plane magnetic field confirm in-plane magnetization of the samples. The details of sample deposition procedure, RHEED patterns, and the hysteresis loops are presented in the Supplemental Materials [28]. The increasing trend of saturation magnetization with x qualitatively follows the Slater-Pauling curve but does not attain the bulk value of saturation magnetization, as expected for Heusler alloy thin films [30]. The ultrafast magnetization dynamics was measured using a two-color all-optical time-resolved magneto-optical Kerr effect (TRMOKE) magnetometer [31] at a fixed probe (wavelength, $\lambda = 800$ nm) fluence of 0.5 mJ/cm^2, while the pump ($\lambda = 400$ nm) fluence has been varied between 3.2 and 9.5 mJ/cm^2. The details of the TRMOKE technique are presented in the Supplemental Materials [28].

III. ULTRAFAST DEMAGNETIZATION

Figure 2(a) shows the ultrafast demagnetization curves with different x values for a fixed pump fluence = 9.5 mJ/cm^2. We have found the relative variation of the transient reflectivity is nearly two orders of magnitude smaller than the relative variation of transient Kerr rotation in our samples, which indicates that the contribution of optical effects to transient Kerr rotation is negligible here [32] (see also Supplemental Materials [28]). The experimental data are fitted using a rate equation derived from the three-temperature model (see Ref. [28]) to extract the ultrafast demagnetization time (τ_M) and fast relaxation time [25]. The τ_M values are plotted as a function of x in Fig. 2(b), which show a slight initial increment followed by a sharp decrement with

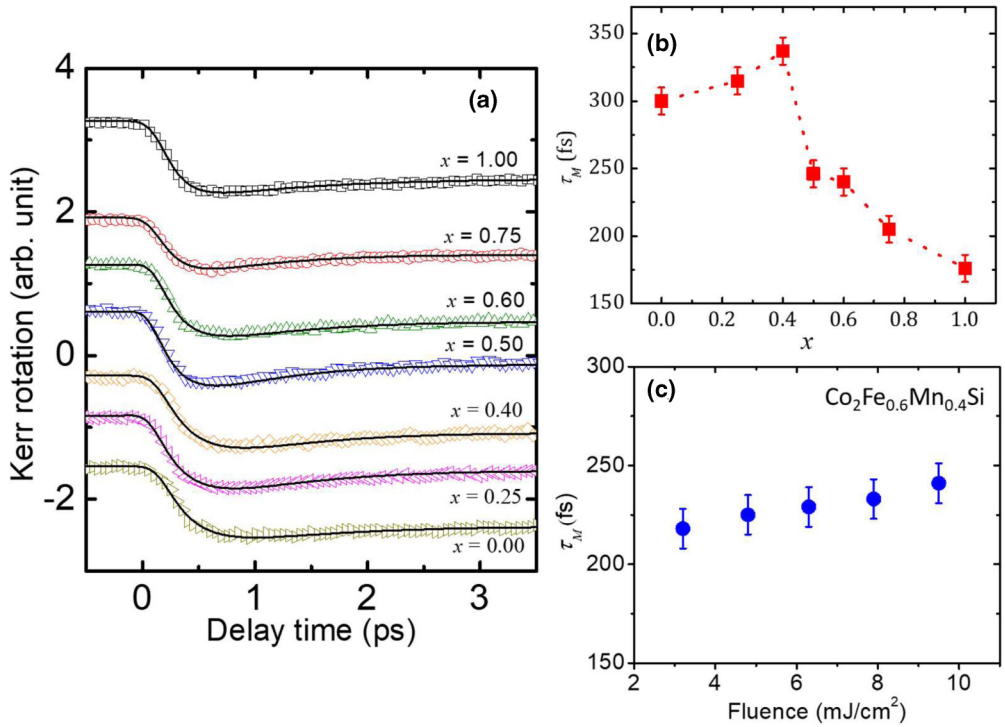

FIG. 2. (a) Ultrafast demagnetization curves for the samples with different alloy composition (x) measured using TRMOKE. Scattered symbols are the experimental data and solid lines are fit using Eq. (1S) of Supplemental Materials [28]. (b) Evolution of τ_M with x at pump fluence of 9.5 mJ/cm^2. Symbols are experimental results and dashed line is a guide to the eye. (c) Variation in τ_M with pump fluence.

x. In addition, the ultrafast demagnetization rate is found to be slower in the present Heusler alloys than in the 3d ferromagnetic metals [9,33]. The extracted τ_M for Co_2MnSi ($x = 0$) and Co_2FeSi ($x = 1$) are 300 and 176 fs, respectively, which are in good agreement with the reported values [10]. The theoretical calculation of electronic band structure of CFMS showed no discernible change in the amount of energy gap in the minority spin band but a change in position of E_F with x, which lies at the two extreme ends of the gap for $x = 0$ and $x = 1$ [34,35]. Thus, at these two points the MSDOS becomes very large close to the Fermi level, while it moves well into the band gap for intermediate x values. As x increases from 0 to 1, the number of valence electrons increases. These additional electrons fill the strongly dispersive majority d states. Consequently, MSDOS shifts with respect to the Fermi energy such that the Fermi level moves from the top of the minority valence band to the bottom of the conduction band. In concurrence, the corresponding total density of states (DOS) varies nonmonotonically. For low x, the DOS is high but it decreases as the Fermi level moves away from the minority valence band. The DOS becomes minimum at $x = 0.4$, followed by gradual increment up to $x = 1$. This nonmonotonic behavior warrants the investigation of ultrafast demagnetization with continuously varying x from 0 to 1. However, a majority of earlier investigations [10,11,36], being focused only on Co_2MnSi ($x = 0$) and Co_2FeSi ($x = 1$), lack a convincing conclusion about the role of Fermi-level position on ultrafast demagnetization mechanism in Heusler alloy. Figure 2(b) clearly shows that τ_M varies with DOS at the Fermi level in a commensurate fashion [36], the reason of which we explain in details below.

In case of 3d transition-metal ferromagnets, the Elliott-Yafet (EY)-based SFS mechanism is believed to be responsible for rapid rise in the spin temperature and ultrafast demagnetization [15]. In this theory it has been shown that a scattering event of an excited electron with a phonon changes the probability to find that electron in one of the spin states, namely the majority spin-up (↑) or minority spin-down (↓) state, thereby delivering angular momentum to the lattice from the electronic system. It arises from the band mixing of majority and minority spin states with similar energy value near the Fermi surface owing to the spin-orbit coupling (SOC). The spin-mixing parameter (b^2) from the EY theory [37,38], derived under various approximations such as a paramagnetic metal, nearly constant electron-phonon matrix element, and no phonon dispersion spectrum, is given by

$$\langle b^2 \rangle = \overline{\min\left(\langle \psi_k|\uparrow\rangle\langle\uparrow|\psi_k\rangle, \langle \psi_k|\downarrow\rangle\langle\downarrow|\psi_k\rangle\right)}, \qquad (1)$$

where ψ_k represents the eigenstate of a single electron and the bar denotes a defined average over all electronic states involved in the EY scattering processes. This equation represents that the spin mixing due to SFS between spin-up and spin-down states depends on the number of spin-up (↑) and spin-down (↓) states at the Fermi level. The spin-mixing parameter in nonequilibrium would not be the same as that in the equilibrium regime and thus, one may not directly relate it to the DOS at the Fermi level in equilibrium. As the spin-mixing parameter in the strong nonequilibrium regime is approximately different by a factor of 2 from that in the equilibrium regime [13], we believe a qualitative comparison between equilibrium density of states and nonequilibrium spin-mixing parameter of different samples is possible.

Consequently, a compact differential equation for the rate of ultrafast demagnetization dynamics as derived by Koopmans *et al.* [38] is given below:

$$\frac{dm}{dt} = Rm\frac{T_p}{T_C}\left(1 - \coth\left(\frac{mT_C}{T_e}\right)\right), \tag{2}$$

where $m = M/M_S$, and T_p, T_C, and T_e denote the phonon temperature, Curie temperature, and electronic temperature, respectively. R is a material specific scaling factor [39], which is calculated to be

$$R = \frac{8a_{sf}T_C^2 g_{ep}}{k_B T_D^2 D_S}, \tag{3}$$

where a_{sf}, g_{ep}, and D_S represent the SFS probability, coupling between electron and phonon subsystems, and magnetic moment divided by the Bohr magneton (μ_B), whereas T_D is the Debye temperature and k_B represents the Boltzmann constant. Further, the expression for g_{ep} is $g_{ep} = \frac{3\pi D_F^2 D_P k_B T_D \lambda_{ep}^2}{2\hbar}$, where D_P and λ_{ep} denote the number of polarization states of spins and electron-phonon coupling constant, respectively, and $\hbar$ is the reduced Planck's constant. Moreover, the ultrafast demagnetization time at low fluence limit can be derived under various approximations as

$$\tau_M = \frac{C_0 F(T/T_C)\hbar}{\pi D_F^2 \lambda_{si}^2 k_B T_C}, \tag{4}$$

where $C_0 = 1/4$, λ_{si} is a factor scaling with impurity concentration, and $F(T/T_C)$ is a function solely dependent on (T/T_C) [40].

Earlier, it has been shown that a negligible D_F in CrO_2 is responsible for large ultrafast demagnetization time. The theoretical calculation for CFMS by Oogane *et al.* shows that D_F initially decreases and then increases with x [41] having a minima at $x = 0.4$. As D_F decreases, the number of effective minority spin states become less, reducing both SOC strength, as shown by Mavropoulos *et al.* [42], and the effective spin-mixing parameter as given by Eq. (1), and vice versa. This will result in a reduced SFS probability and rate of ultrafast demagnetization. In addition, the decrease in D_F makes g_{ep} weaker, which, in turn, reduces the value of R as evident from Eq. (3). As the value of R diminishes, it will slow down the rate of ultrafast demagnetization which is clear from Eq. (2). In essence, a lower value of D_F indicates a lower value of R, i.e., slower demagnetization rate and longer ultrafast demagnetization time. Thus, ultrafast demagnetization time is highest for $x = 0.4$. On both sides of $x = 0.4$, the value of R will increase and ultrafast demagnetization time will decline continuously. Our experimental results, supported by the existing theoretical results for the CFMS samples with varying alloy composition, clearly show that the position of Fermi level is a decisive factor for the rate of ultrafast demagnetization. This happens due to the continuous tunability of D_F with x, which causes an ensuing variation in the number of scattering channels available for SFS. To capture the effect of pump fluence on the variation of τ_M, we have measured the ultrafast demagnetization curves for various applied pump fluences. All the fluence-dependent ultrafast demagnetization curves are analyzed and the values of corresponding τ_M are extracted. The change in τ_M with fluence is shown in Fig. 2(c). A slight change of about 10% in τ_M with fluence is observed which is negligible in comparison to the change (∼100%) of τ_M with x. However, this increment with fluence can be explained using the enhanced spin fluctuations at much higher elevated temperature of the spin system [39]. We also found out that the relaxation rate increases as the Fermi level moves away from the minority valence band, which agrees well with the earlier studies [43].

IV. MAGNETIC DAMPING

As the primary microscopic channel for spin angular momentum transfer is the same for both ultrafast demagnetization and magnetic damping, it is expected to find a correlation between them. We have measured the time-resolved Kerr rotation data corresponding to the magnetization precession at an applied in-plane bias magnetic field (H_b) of 3.5 kOe as shown in Fig. 3(a). Unfortunately, we could not induce precessional motion in the sample with $x = 0.25$, which was probably due to the degraded structural quality. The macrospin modeling is employed to analyze the time-dependent precessional data obtained by solving the Landau-Lifshitz-Gilbert equation [44] which is given below:

$$\frac{d\hat{m}}{dt} = -\gamma(\hat{m} \times H_{eff}) + \alpha\left(\hat{m} \times \frac{d\hat{m}}{dt}\right), \tag{5}$$

where γ is the gyromagnetic ratio and is related to Landé g factor by $\gamma = g\mu_B/\hbar$. H_{eff} is the total effective magnetic field consisting of H_b, exchange field (H_{ex}), dipolar field (H_{dip}), and anisotropy field (H_K). The experimental variation of precession frequency (f) against H_b is fitted with the Kittel formula for uniform precession to extract H_K values. The details of the fit are discussed in the Supplemental Materials [28].

For evaluation of α, all the measured data representing single-frequency oscillation are fitted with a general damped sine-wave equation superimposed on a biexponential decay function, which is given as

$$M(t) = A + B_1 e^{-t/\tau_{fast}} + B_2 e^{-t/\tau_{slow}} + M(0)e^{-t/\tau}\sin(\omega t - \zeta), \tag{6}$$

where ζ is the initial phase of oscillation and τ is the precessional relaxation time. τ_{fast} and τ_{slow} are the fast and slow relaxation times, representing the rate of energy transfer in between different energy baths (electron, spin, and lattice) following the ultrafast demagnetization and the energy transfer rate between the lattice and surrounding, respectively. A, B_1, and B_2 are constant coefficients. The value of α is extracted by further analyzing τ using

$$\alpha = \frac{2}{[\gamma\tau(2H_b\cos(\delta - \varphi) + H_1 + H_2)]}, \tag{7}$$

where $H_1 = 4\pi M_S + \frac{2K_\perp}{M_S} - \frac{2K_1\sin^2\varphi}{M_S} + \frac{K_2(2-\sin^2(2\varphi))}{M_S}$ and $H_2 = \frac{2K_1\cos(2\varphi)}{M_S} + \frac{2K_2\cos(4\varphi)}{M_S}$. Here δ and φ represent the angles of H_b and in-plane equilibrium M with respect to the CFMS [110] axis [44]. The uniaxial, biaxial, and out-of-plane magnetic anisotropies are denoted as K_1, K_2, and $K_\perp$, respectively. In our case K_2 has a reasonably large value while K_1 and $K_\perp$ are negligibly small. Plugging in all parameters including

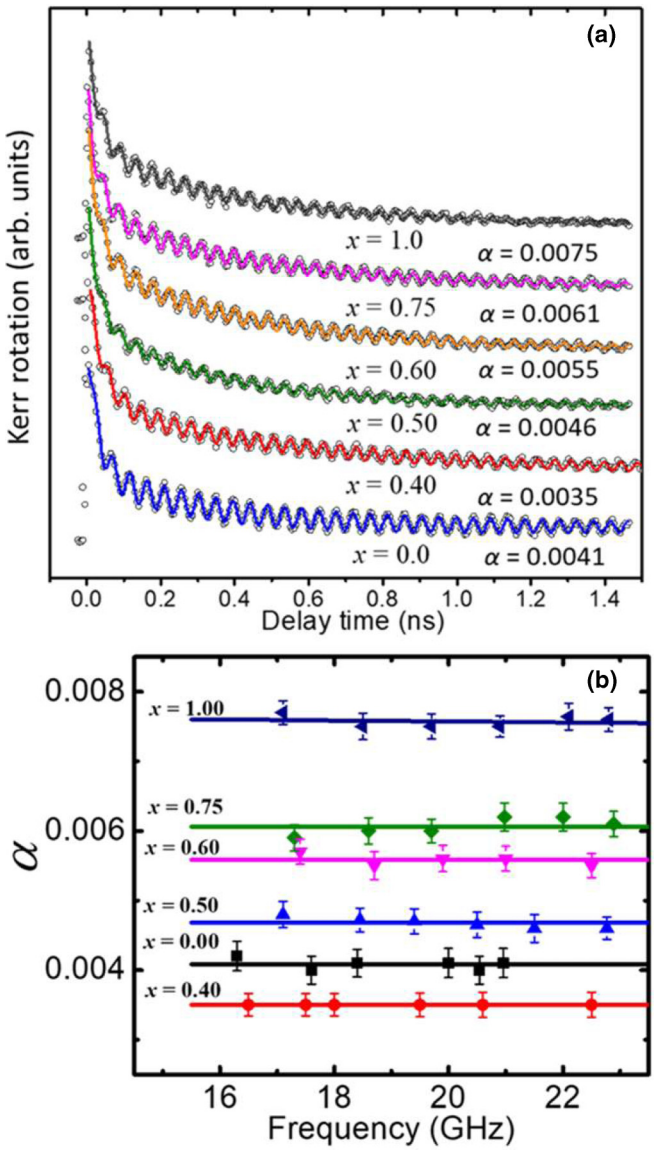

FIG. 3. (a) Time-resolved Kerr rotation data showing precessional dynamics for samples with different x values. Symbols are the experimental data and solid lines are fit with damped sine wave equation [Eq. (6)]. The extracted α values are given below every curve. (b) Variation of α with precession frequency (f) for all samples as shown by symbols, while solid lines are linear fit.

the magnetic anisotropy constant K_2 in Eq. (7), we have obtained the values of α to be 0.0041, 0.0035, 0.0046, 0.0055, 0.0061, and 0.0075 for $x = 0.00$, 0.40, 0.50, 0.60, 0.75, and 1.00, respectively. The α values are extracted directly from the decaying profile of the precession amplitude, which is somewhat different from the one extracted from ferromagnetic resonance linewidth. Figure 3(b) shows the variation of α with frequency for all the samples. For each sample, α remains constant with frequency, which rules out the presence of extrinsic mechanisms contributing to the α. Next, we focus on the variation of α with x. Our experimental results show a nonmonotonic variation of α with x with a minima at $x = 0.4$, which is exactly opposite to the variation of τ_M with x. On the basis of Kambersky's SFS model [45], α is governed by the spin-orbit interaction and can be expressed as

$$\alpha = \frac{\gamma\hbar^2(\delta g)^2}{4\Gamma M_S} D_F, \tag{8}$$

where δg and Γ^{-1} represent the deviation of g factor from free-electron value ($\sim$2.0) and ordinary electron-phonon collision frequency. Equation (8) suggests that α is directly proportional to D_F and thus it becomes minimum when D_F is minimum. This leads to the nonmonotonic variation of α, which agrees well with earlier observation [41]. To eliminate the possible effects of γ and M_S, we have plotted the variation of relaxation frequency, $G = \alpha\gamma M_S$ with x which also exhibits similar variation as α (see the Supplemental Materials [28]).

V. CORRELATION BETWEEN ULTRAFAST DEMAGNETIZATION AND DAMPING

Finally, to explore the correlation between α, τ_M, and alloy composition, we have plotted these quantities against x as shown in Fig. 4(a). We observe that τ_M and α vary in opposite manner with x, having their respective maxima and minima at $x = 0.4$. However, they do not possess a mirror symmetry. Although τ_M and α refer to two different timescales, both of them follow the trend of variation of D_F with x. This shows that the alloy composition-controlled Fermi-level tunability and the ensuing SFS are responsible for both ultrafast demagnetization and Gilbert damping. Figure 4(b) represents the variation of τ_M with inverse of α. An approximately linear trend in Fig. 4(b) establishes an inversely proportional relation between them. We believe that this connection in between ultrafast demagnetization and damping is bridged by the density of states-dependent spin-flip scattering rate. The latter varies as a function of alloy composition-dependent Fermi level as shown in Figs. 4(c) and 4(d). As D_F increases (decreases), it offers more (less) scattering channels for both the ultrafast demagnetization as well as angular momentum dissipation responsible for damping which results in shorter (longer) demagnetization time and higher (lower) damping constant. Initially, under the assumption of two different magnetic fields, i.e., exchange field and total effective magnetic field, Koopmans *et al.* theoretically proposed that Gilbert damping parameter and ultrafast demagnetization time are inversely proportional [38]. However, that raised intense debate and in 2010, when Fähnle *et al.* showed that α can either be proportional or inversely proportional to τ_M depending upon the dominating microscopic contribution to the magnetic damping [46]. This was later experimentally demonstrated in Co/Ni multilayers by Zhang *et al.* [47]. The linear relation sustains when the damping is dominated by conductivitylike contribution, whereas the resistivitylike contribution leads to an inverse relation. The basic difference between the conductivitylike and the resistivitylike contributions lies in the angular momentum transfer mechanism via electron-hole (e-h) pair generation. The generation of e-h pair in the same band, i.e., intraband mechanism, leads to the conductivitylike contribution. On the contrary, when e-h pair is generated in different bands (interband mechanism), the contribution is dominated by resistivity. Our observation of the inversely proportional relation between α and τ_M clearly indicates that in case of the CFMS Heusler alloy systems, the damping is dominated by

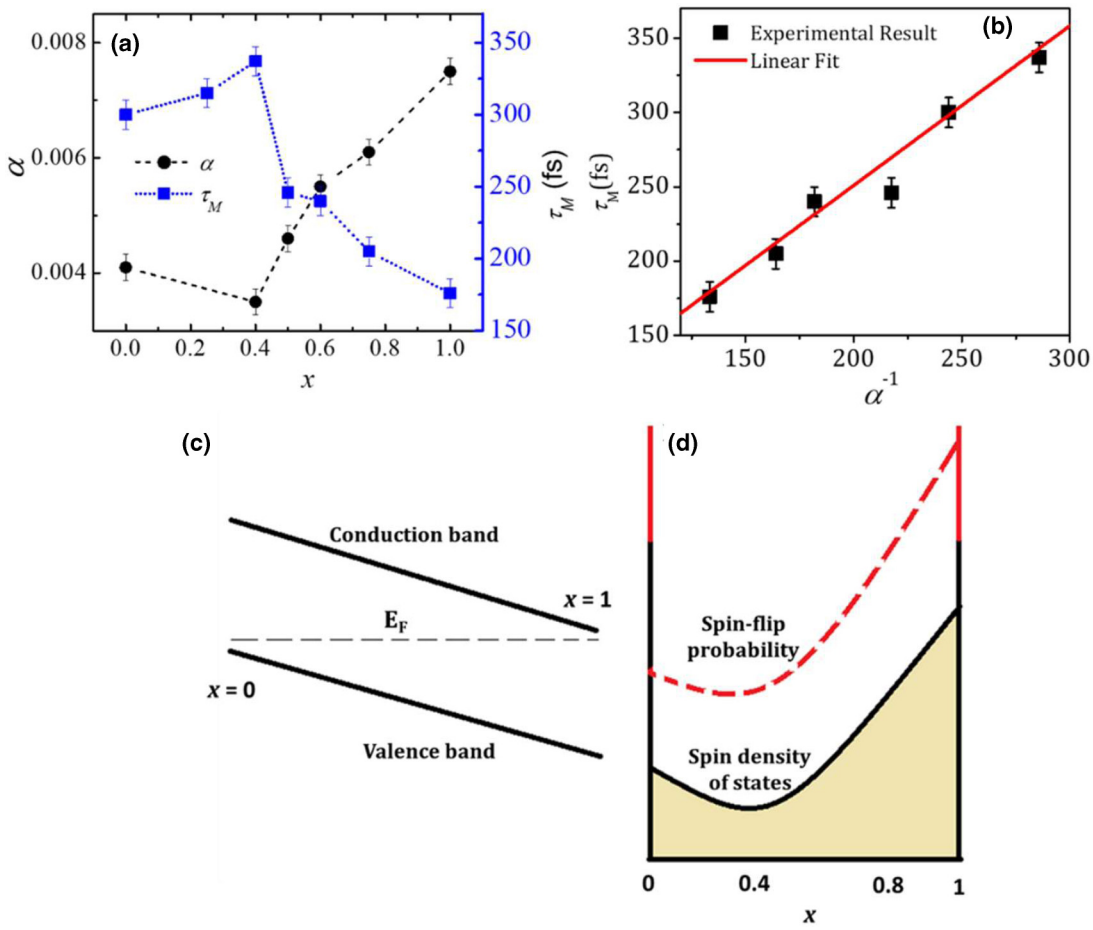

FIG. 4. (a) Variation of τ_M and α with x. Square and circular symbols denote the experimental results, and dashed, dotted lines are guide to eye. (b) Variation of τ_M with α^{-1}. Symbols represent the experimentally obtained values and solid line refers to linear fit. Schematic showing (c) the variation of the position of the Fermi level within the band gap of minority spin band and (d) the variation of spin density of states and resulting spin-flip probability against x.

resistivitylike contribution arising from interband *e-h* pair generation. This is in contrast to the case of Co, Fe, and Ni, where the conductivity contribution dominates [48]. Typical resistivity (ρ) values for Co_2MnSi ($x = 0$) are $5\,\mu\Omega\,cm$ at 5 K and $20\,\mu\Omega\,cm$ at 300 K [49]. The room temperature value of ρ corresponds to an order of magnitude larger contribution of the interband *e-h* pair generation than the intraband generation [48]. This is in strong agreement with our experimental results and their conclusion. This firmly establishes that unlike conventional transition metal ferromagnets, damping in CFMS Heusler alloys is dominated by resistivitylike contribution, which results in an inversely proportional relation between α and τ_M.

VI. CONCLUSIONS

In summary, we have investigated the ultrafast demagnetization and magnetic Gilbert damping in the CFMS Heusler alloy system with varying alloy composition (x), ranging from $x = 0$ (CMS) to $x = 1$ (CFS) and identified a strong correlation between τ_M and x, the latter controlling the position of Fermi level within the minority band gap. We have found that τ_M varies nonmonotonically with x, having a maximum value of ~350 fs for $x = 0.4$ corresponding to the lowest D_F and highest degree of spin polarization. In-depth investigation has revealed that the ultrafast demagnetization process in CFMS is primarily governed by the composition-controlled variation in spin-flip scattering rate due to variable D_F. Furthermore, we have systematically investigated the precessional dynamics with variation in x and extracted the value of α from there. Our results have led to a systematic correlation in between τ_M, α, and x and we have found an inversely proportional relationship between τ_M and α. Our thorough investigation across the alloy composition ranging from CMS to CFS has firmly established the fact that both ultrafast demagnetization and magnetic Gilbert damping in CFMS are strongly controlled by the spin density of states at the Fermi level. Therefore, our study has enlightened a path for qualitative understanding of spin polarization from ultrafast demagnetization time as well as magnetic Gilbert damping and led a step forward for ultrafast magnetoelectronic device applications.

ACKNOWLEDGMENTS

This work was funded by S. N. Bose National Centre for Basic Sciences under Projects No. SNB/AB/12-13/96, No.

SNB/AB/18-19/211 and Grant-in-Aid for Scientific Research (A) (Grant No. JP20H00299) from JSPS KAKENHI, Japan. The structural characterization was partly carried out at the Cooperative Research and Development Center for Advanced Materials, IMR, Tohoku University.

[1] T. Kubota, S. Tsunegi, M. Oogane, S. Mizukami, T. Miyazaki, H. Naganuma, and Y. Ando, Appl. Phys. Lett. **94**, 122504 (2009).
[2] A. Hirohata and K. Takanashi, J. Phys. D: Appl. Phys. **47**, 193001 (2014).
[3] R. J. Soulen, J. M. Byers, M. S. Osofsky, B. Nadgorny, T. Ambrose, S. F. Cheng, C. T. Broussard, P. R. Tanaka, J. Nowak, J. S. Moodera, A. Barry, and J. M. D. Coey, Science **282**, 85 (1998).
[4] I. I. Mazin, Phys. Rev. Lett. **83**, 1427 (1999).
[5] K. E. H. M. Hanssen, P. E. Mijnarends, L. P. L. M. Rabou, and K. H. J. Buschow, Phys. Rev. B **42**, 1533 (1990).
[6] L. Ritchie, G. Xiao, Y. Ji, T. Y. Chen, C. L. Chien, M. Zhang, J. Chen, Z. Liu, G. Wu, and X. X. Zhange, Phys. Rev. B **68**, 104430 (2003).
[7] D. T. Pierce and F. Meier, Phys. Rev. B **13**, 5484 (1976).
[8] Q. Zhang, A. V. Nurmikko, G. X. Miao, G. Xiao, and A. Gupta, Phys. Rev. B **74**, 064414 (2006).
[9] G. M. Müller, J. Walowski, M. Djordjevic, G. -X. Miao, A. Gupta, A. V. Ramios, K. Gehrke, V. Moshnyaga, K. Samwer, J. Schmalhorst, A. Thomas, A. Hütten, G. Reiss, J. S. Moodera, and M. Münzenberg, Nat. Mater. **8**, 56 (2009).
[10] D. Steil, S. Alebrand, T. Roth, M. Krauβ, T. Kubota, M. Oogane, Y. Ando, H. C. Schneider, M. Aeschlimann, and M. Cinchetti, Phys. Rev. Lett. **105**, 217202 (2010).
[11] A. Mann, J. Walowski, M. Münzenberg, S. Maat, M. J. Carey, J. R. Childress, C. Mewes, D. Ebke, V. Drewello, G. Reiss, and A. Thomas, Phys. Rev. X **2**, 041008 (2012).
[12] E. Beaurepaire, J. C. Merle, A. Daunois, and J.-Y. Bigot, Phys. Rev. Lett. **76**, 4250 (1996).
[13] K. Carva, M. Battiato, and P. M. Oppeneer, Phys. Rev. Lett. **107**, 207201 (2011).
[14] D. Steiauf and M. Fähnle, Phys. Rev. B **79**, 140401(R) (2009).
[15] M. Cinchetti, M. Sánchez Albaneda, D. Hoffmann, T. Roth, J.-P. Wüstenberg, M. Krauß, O. Andreyev, H. C. Schneider, M. Bauer, and M. Aeschlimann, Phys. Rev. Lett. **97**, 177201 (2006).
[16] M. Battiato, K. Carva, and P. M. Oppeneer, Phys. Rev. Lett. **105**, 027203 (2010).
[17] A. Eschenlohr, M. Battiato, P. Maldonado, N. Pontius, T. Kachel, K. Holldack, R. Mitzner, A. Fohlisch, P. M. Oppeneer, and C. Stamm, Nat. Mater. **12**, 332 (2013).
[18] D. Rudolf, C. L. Vorakiat, M. Battiato, R. Adam, J. M. Shaw, E. Turgut, P. Maldonado, S. Mathias, P. Grychtol, H. T. Nembach, T. J. Silva, M. Aeschlimann, H. C. Kapteyn, M. M. Murnane, C. M. Schneider, and P. M. Oppeneer, Nat. Commun. **3**, 1037 (2012).
[19] U. Atxitia, O. Chubykalo-Fesenko, J. Walowski, A. Mann, and M. Münzenberg, Phys. Rev. B **81**, 174401 (2010).
[20] Z. Chen and L.-W. Wang, Sci. Adv. **5**, eaau8000 (2019).
[21] P. Tengdin, C. Gentry, A. Blonsky, D. Zusin, M. Gerrity, L. Hellbruck, M. Hofherr, J. Shaw, Y. Kvashnin, E. K. Delczeg-czirjak, M. Arora, H. Nembach, T. J. Silva, S. Mathias, M. Aeschlimann, H. C. Kapteyn, D. Thonig, K. Koumpouras, O. Eriksson, and M. M. Murnane, Sci. Adv. **6**, eaaz1100 (2020).
[22] M. Hofherr, S. Hauser, J. K. Dewhurst, P. Tengdin, S. Sakshath, H. T. Nembach, S. T. Weber, J. M. Shaw, T. J. Silva, H. C. Kapteyn, M. Cinchetti, B. Rethfeld, M. M. Murnane, D. Steil, B. Stadtmuller, S. Sharma, M. Aeschlimann, and S. Mathias, Sci. Adv. **6**, eaay8717 (2020).
[23] Y. Miura, K. Nagao, and M. Shirai, Phys. Rev. B **69**, 144413 (2004).
[24] L. Bainsla, A. I. Mallick, M. M. Raja, A. K. Nigam, B. S. D. C. S. Varaprasad, Y. K. Takahashi, A. Alam, K. G. Suresh, and K. Hono, Phys. Rev. B **91**, 104408 (2015).
[25] G. Malinowski, F. Dalla Longa, J. H. H. Rietjens, P. V. Paluskar, R. Huijink, H. J. M. Swagten, and B. Koopmans, Nat. Phys. **4**, 855 (2008).
[26] S. Pan, S. Mondal, T. Seki, K. Takanashi, and A. Barman, Phys. Rev. B **94**, 184417 (2016).
[27] S. Pan, T. Seki, K. Takanashi, and A. Barman, Phys. Rev. Appl. **7**, 064012 (2017).
[28] See Supplemental Materials at http://link.aps.org/supplemental/10.1103/PhysRevB.101.224412 for sample preparation method, detailed analysis of XRD peak intensity ratio, RHEED images, hysteresis loops, analyses of ultrafast demagnetization time and relaxation time, variation of precession frequency with external bias magnetic field, and the variation of relaxation frequency as a function of alloy composition.
[29] Y. Takamura, R. Nakane, and S. Sugahara, J. Appl. Phys. **105**, 07B109 (2009).
[30] I. Galanakis, P. H. Dederichs, and N. Papanikolaou, Phys. Rev. B **66**, 174429 (2002).
[31] S. Panda, S. Mondal, J. Sinha, S. Choudhury, and A. Barman, Sci. Adv. **5**, eaav7200 (2019).
[32] E. Carpene, F. Boschini, H. Hedayat, C. Piovera, C. Dallera, E. Puppin, M. Mansurova, M. Munzenberg, X. Zhang, and A. Gupta, Phys. Rev. B **87**, 174437 (2013).
[33] J. Walowski and M. Munzenberg, J. Appl. Phys. **120**, 140901 (2016).
[34] B. Balke, G. H. Fecher, H. C. Kandpal, C. Felser, K. Kobayashi, E. Ikenaga, J.-J. Kim, and S. Ueda, Phys. Rev. B **74**, 104405 (2006).
[35] Y. Sakuraba, S. Kokado, Y. Hirayama, T. Furubayashi, H. Sukegawa, S. Li, Y. K. Takahashi, and K. Hono, Appl. Phys. Lett. **104**, 172407 (2014).
[36] D. Steil, O. Schmitt, R. Fetzer, T. Kubota, H. Naganuma, M. Oogane, Y. Ando, A. K. Suszka, O. Idigoras, and G. Wolf, New J. Phys. **16**, 063068 (2014).
[37] R. J. Elliott, Phys. Rev. **96**, 266 (1954).
[38] B. Koopmans, G. Malinowski, F. Dalla Longa, D. Steiauf, M. Fähnle, T. Roth, M. Cinchetti, and M. Aeschlimann, Nat. Mater. **9**, 259 (2010).
[39] K. C. Kuiper, T. Roth, A. J. Schellekens, O. Schmitt, B. Koopmans, M. Cinchetti, and M. Aeschlimann, Appl. Phy. Lett. **105**, 202402 (2014).
[40] B. Koopmans, J. J. M. Ruigrok, F. Dalla Longa, and W. J. M. de Jonge, Phys. Rev. Lett. **95**, 267207 (2005).
[41] M. Oogane, T. Kubota, Y. Kota, S. Mizukami, H. Naganuma, A. Sakuma, and Y. Ando, Appl. Phys. Lett. **96**, 252501 (2010).

[42] P. Mavropoulos, K. Sato, R. Zeller, P. H. Dederichs, V. Popescu, and H. Ebert, Phys. Rev. B **69**, 054424 (2004).
[43] J. P. Wüstenberg, D. Steil, S. Alebrand, T. Roth, M. Aeschlimann, and M. Cinchetti, Phys. Status Solidi B **248**, 2330 (2011).
[44] S. Qiao, S. Nie, J. Zhao, and X. Zhang, Appl. Phys. Lett. **105**, 172406 (2014).
[45] V. Kamberský, Can. J. Phy. **48**, 2906 (1970).
[46] M. Fähnle, J. Seib, and C. Illg, Phys. Rev. B **82**, 144405 (2010).
[47] W. Zhang, W. He, X.-Q. Zhang, Z.-H. Cheng, J. Teng, and M. Fahnle, Phys. Rev. B **96**, 220415(R) (2017).
[48] K. Gilmore, Y. U. Idzerda, and M. D. Stiles, Phys. Rev. Lett. **99**, 027204 (2007).
[49] C. Liu, C. K. A. Mewes, M. Chshiev, T. Mewes, and W. H. Butler, Appl. Phys. Lett. **95**, 022509 (2009).